ARMY RESEARCH LABORATORY

Influence of Metal Substrates on the Detection of Explosive Residues With Laser-Induced Breakdown Spectroscopy

by Jennifer L. Gottfried

ARL-RP-427 **April 2013**

A reprint from *Applied Optics,* Vol. 52, No. 4, pp. B10–B19, 1 February 2013.

NOTICES

Disclaimers

The findings in this report are not to be construed as an official Department of the Army position unless so designated by other authorized documents.

Citation of manufacturer's or trade names does not constitute an official endorsement or approval of the use thereof.

Destroy this report when it is no longer needed. Do not return it to the originator.

Army Research Laboratory
Aberdeen Proving Ground, MD 21005-5069

ARL-RP-427 **April 2013**

Influence of Metal Substrates on the Detection of Explosive Residues With Laser-Induced Breakdown Spectroscopy

Jennifer L. Gottfried
Weapons and Materials Research Directorate, ARL

A reprint from *Applied Optics,* Vol. 52, No. 4, pp. B10–B19, 1 February 2013.

REPORT DOCUMENTATION PAGE

Form Approved
OMB No. 0704-0188

1. REPORT DATE *(DD-MM-YYYY)*	2. REPORT TYPE	3. DATES COVERED (From - To)
April 2013	Reprint	June 2009–February 2012

4. TITLE AND SUBTITLE
Influence of Metal Substrates on the Detection of Explosive Residues With Laser-Induced Breakdown Spectroscopy

5a. CONTRACT NUMBER

5b. GRANT NUMBER

5c. PROGRAM ELEMENT NUMBER

6. AUTHOR(S)
Jennifer L. Gottfried

5d. PROJECT NUMBER

5e. TASK NUMBER

5f. WORK UNIT NUMBER

7. PERFORMING ORGANIZATION NAME(S) AND ADDRESS(ES)
U.S. Army Research Laboratory
ATTN: RDRL-WML-B
Aberdeen Proving Ground, MD 21005-5069

8. PERFORMING ORGANIZATION REPORT NUMBER
ARL-RP-427

9. SPONSORING/MONITORING AGENCY NAME(S) AND ADDRESS(ES)

10. SPONSOR/MONITOR'S ACRONYM(S)

11. SPONSOR/MONITOR'S REPORT NUMBER(S)

12. DISTRIBUTION/AVAILABILITY STATEMENT
Approved for public release; distribution is unlimited.

13. SUPPLEMENTARY NOTES
A reprint from *Applied Optics*, Vol. 52, No. 4, pp. B10–B19, 1 February 2013.

14. ABSTRACT
Laser-induced breakdown spectroscopy is a promising approach for explosive residue detection, but several limitations to its widespread use remain. One issue is that the emission spectra of the residues are dependent on the substrate composition because some of the substrate is usually entrained in the laser-induced plasma and the laser–material interaction can be significantly affected by the substrate type. Here, we have demonstrated that despite the strong spectral variation in cyclotrimethylenetrinitramine (RDX) residues applied to various metal substrates, classification of the RDX residue independent of substrate type is feasible. Several approaches to improving the chemometric models based on partial least squares discriminant analysis (PLS-DA) have been described: classifying the RDX residue spectra together in one class independent of substrate, using selected emission intensities and ratios to increase the true positive rate (TPR) and decrease the false positive rate (FPR), and fusing the results from two PLS-DA models generated using the full broadband spectra and selected intensities and ratios. The combination of these approaches resulted in a TPR of 97.5% and a FPR of 1.0% for RDX classification on metal substrates.

15. SUBJECT TERMS
LIBS, RDX, metal, chemometrics

16. SECURITY CLASSIFICATION OF:			17. LIMITATION OF ABSTRACT	18. NUMBER OF PAGES	19a. NAME OF RESPONSIBLE PERSON
a. REPORT	b. ABSTRACT	c. THIS PAGE			Jennifer L. Gottfried
Unclassified	Unclassified	Unclassified	UU	16	19b. TELEPHONE NUMBER (*Include area code*) 410-278-7573

Influence of metal substrates on the detection of explosive residues with laser-induced breakdown spectroscopy

Jennifer L. Gottfried

U.S. Army Research Laboratory, RDRL-WML-B, Aberdeen Proving Ground, Maryland 21005, USA (jennifer.gottfried@us.army.mil)

Received 14 August 2012; accepted 5 September 2012;
posted 11 September 2012 (Doc. ID 174360); published 18 October 2012

Laser-induced breakdown spectroscopy is a promising approach for explosive residue detection, but several limitations to its widespread use remain. One issue is that the emission spectra of the residues are dependent on the substrate composition because some of the substrate is usually entrained in the laser-induced plasma and the laser–material interaction can be significantly affected by the substrate type. Here, we have demonstrated that despite the strong spectral variation in cyclotrimethylenetrinitramine (RDX) residues applied to various metal substrates, classification of the RDX residue independent of substrate type is feasible. Several approaches to improving the chemometric models based on partial least squares discriminant analysis (PLS-DA) have been described: classifying the RDX residue spectra together in one class independent of substrate, using selected emission intensities and ratios to increase the true positive rate (TPR) and decrease the false positive rate (FPR), and fusing the results from two PLS-DA models generated using the full broadband spectra and selected intensities and ratios. The combination of these approaches resulted in a TPR of 97.5% and a FPR of 1.0% for RDX classification on metal substrates.

OCIS codes: 280.0280, 280.1545, 280.3420, 300.6365.

1. Introduction

Interest in explosive residue detection for military and civilian applications continues to fuel new research in this challenging area. Laser-induced breakdown spectroscopy (LIBS) is a promising approach for this problem because of its many advantages, including the ability to do standoff detection, the capability for real-time analysis of targets with no sample preparation, and the strong signal compared to other laser-based methods such as Raman spectroscopy and laser-induced fluorescence [1]. In LIBS, a pulsed laser is focused on the sample surface and ablates a small amount of material (typically nanograms or less) [2]. The atomization and ionization of the ablated material results in the formation of a laser-induced plasma that emits radiation characteristic of the ablated material. Depending on the laser energy and pulse duration, the laser-induced plasma can last hundreds of microseconds; during this time, chemical reactions occur in the plasma that can affect the emission spectrum [3–9]. For residue detection, the substrate material is often ablated by the laser as well, and the resulting matrix effects can alter the emission spectrum. A recent review described some of the challenges of quantitative LIBS because of matrix effects [10], but even for qualitative applications such as material identification, matrix effects must be compensated for as they can significantly alter the spectroscopic signature of the material [9,11–16].

Previous studies at the U.S. Army Research Laboratory (ARL) have primarily focused on the detection of explosive residues on a single type of substrate (aluminum [17] or painted surfaces [18]). Other researchers, using either an aluminum substrate or sampling bulk explosive, have explored the effects of laser wavelength [19,20], pulse energy [6], and atmospheric influence [4,6] for explosive

detection. More recently, we have investigated the effect of chemical reactions involving metal particles and the explosive cyclotrimethylenetrinitramine (RDX) in the laser-induced plasma on the LIBS signature [9]. In addition to matrix effects induced by the interaction of the laser with the metal substrate (affecting the amount of material ablated, plasma temperatures, electron densities, etc.), we demonstrated that differences in the plasma chemistry of RDX with the ablated metals significantly alters the LIBS spectra of RDX. While organic substrates such as painted surfaces present a challenge because of the presence of key emission features for the identification of explosives (C, H, N, O) in the spectra of the substrates themselves, the complex plasma chemistry that occurs with metallic substrates poses a unique challenge for the classification of explosive residues that has not previously been investigated. For this study, we developed partial least squares discriminant analysis (PLS-DA) [21] models in order to determine if the differences observed in the RDX spectra preclude successful classification of the explosive on different metal substrates.

2. Experimental Methods

The spectra analyzed in this paper were acquired for the previous study [9]. Briefly, the experimental setup consisted of two collinear Nd:YAG lasers (Continuum Surelite, 1064 nm, 420 mJ per laser) focused onto the sample surface with a 10 cm lens. A double-pulse laser system was used to both decrease atmospheric entrainment in the plasma and increase the signal-to-noise ratio of the relevant explosive emission features [22,23]. The plasma emission was directed into a 400 μm fiber optic using a pierced mirror setup. An echelle spectrometer (Catalina Scientific EMU-65, resolution $\sim 31,000\ \lambda/\mathrm{FWHM}$) was paired with an electromagnetic CCD detector (Andor iXon, gain = 2) to collect the LIBS spectra (~200–1000 nm) under an argon flow with the following timing parameters: interpulse delay $\Delta t = 2$ μs, gate width $t_{\mathrm{int}} = 50$ μs, and gate delay $t_{\mathrm{delay}} = 1$ μs.

Colleagues at ARL provided Class 1 (<850 μm particle diameter), military-grade RDX. A small quantity of RDX (~mg) was applied to various metal surfaces and spread into a thin layer with a polytetrafluoroethylene tool. Although the amount of RDX adhered to the surfaces was not quantified, in all cases the substrate was visible through the layer of RDX. The substrates used for this experiment included high-purity metal foils obtained from Sigma–Aldrich: Al (99.999%), Cu (99.999%), Ni (99.98%), Sn (99.998%), and Ti (99.998%). Fifty single-shot spectra of RDX residue on each of the pure metal substrates were obtained. Spectra of RDX residue on various samples from our laboratory (unknown compositions representative of contaminated "real-world" substrates) and standard reference materials (SRMs) with precisely known minor constituents purchased from the National Institutes of Standards and Technology (NIST) were also acquired (20 each). An identical number of spectra from each of the blank metals were also recorded. All of the substrates were used as obtained, with no special cleaning procedure. Table 1 lists all the substrates studied.

Although several advanced chemometric techniques have been proven effective for the analysis of LIBS spectra, we have found that PLS-DA works particularly well for explosive residue detection [17]. The single-shot LIBS spectra were used as inputs for the PLS-DA models developed using the PLS_Toolbox version 5.8.3 (Eigenvector Research, Inc.) running under MATLAB version 7.9 (Mathworks). It should be noted that the PLS-DA models calculated based on hundreds of broadband LIBS spectra (40,001 intensity channels each) could not be calculated with earlier versions of the MATLAB software, as these calculations are computationally expensive and require efficient algorithms for the relevant matrix operations. The full broadband spectra were normalized to a maximum spectral intensity equal to one and mean-centered prior to PLS-DA analysis. Input variable data sets consisting of selected emission intensities and ratios were autoscaled prior to analysis.

3. Results and Discussion

A. LIBS Spectra

The appearance of spectral features resulting from the RDX residue (e.g., C, CN, H, N, and O) on the high-purity substrates (Al, Cu, Ni, Sn, Ti) was easily observed, despite the presence of hundreds of emission lines due to the metal substrate and argon bath gas (Figure 1). As described in the previous study [9], however, the relative intensities of the emission features of RDX depend quite strongly on the properties of the substrate. For example, CN, which is formed primarily via the reaction of C and N_2, has much weaker emission lines on the Ni substrate

Table 1. List of Pure Metal Substrates and Alloys[a]

High-Purity Substrates	Laboratory Substrates	Metal Alloy Substrates	NIST SRM #
Al (99.999%) (100)	Ag (40)	Al alloy 380 (40)	1256b
Cu (99.999%) (100)	Au (40)	Al alloy 5182 (40)	1715
Ni (99.98%) (100)	In (40)	Al alloy 7075 (40)	1259
Sn (99.998%) (100)	Mg (40)	Ni–Cu alloy (40)	C1248
Ti (99.7%) (100)	Zn (40)	Pb-base alloy (40)	C2417
	Al_2O_3 (40)	High purity Pb alloy (40)	C2418
		Low alloy steel (40)	1761a
		Stainless steel (40)	C1296
		Naval brass B (40)	1107
		Red brass B (40)	1110
		High temp. alloy L-605 (40)	1242
		Ti-base alloy (40)	641
		Zn-base alloy (40)	625

[a]The total number of single-shot spectra acquired, both with and without RDX, is listed in parentheses.

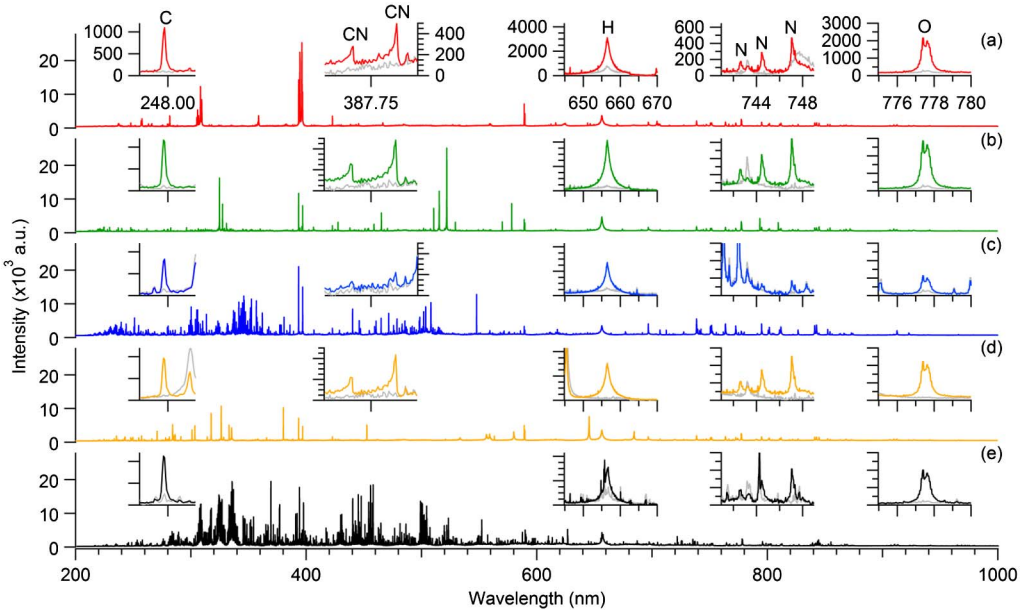

Fig. 1. (Color online) LIBS spectra of RDX residue on high-purity (a) Al, (b) Cu, (c) Ni, (d) Sn, and (e) Ti substrates. The insets show the emission lines due to RDX (C, CN, H, N, and O); the CN lines were not visible for the Ti substrate because of overlapping Ti emission lines. The gray lines in the insets correspond to the relevant blank substrate spectra.

[Fig. 1(c)], despite similar RDX concentrations. Interference from strong Ti lines precludes the observation of CN on the Ti substrate [Fig. 1(e)]. In general, the spectra of the blank high-purity substrates show little evidence of organic residue contamination, and the presence of RDX on the substrate is readily apparent.

Spectra of RDX residue on the laboratory substrates (Ag, Au, In, Mg, Zn), on the other hand, are more difficult to distinguish from the blank substrates (Fig. 2). The exact compositions of the laboratory substrates are not known, but they contain significant emission from C, H, N, and O. Although some surface contamination was possible, the organic signals from the blank substrates persisted even after several successive laser shots into the blank substrate. As with the high-purity substrates, the relative emission intensities due to the RDX residue vary from substrate to substrate. These substrates present a bigger challenge for a model designed to distinguish RDX residue from blank substrates due the emission from organic components in the metals.

Figure 3 shows selected regions from the LIBS spectra from a series of Al-containing substrates. The various alloy and alumina (Al_2O_3) substrates contain numerous emission lines from minor components not present in the high-purity Al sample. These substrates were chosen to test the ability of a model trained on the high-purity Al to identify primarily Al-containing samples. Similarly, selected regions of the other metal-alloy substrate spectra are shown in Fig. 4. Clear differences between similar alloys and their high-purity analogues (Fig. 1) can be observed in the LIBS spectra, presenting a good test for the robustness of PLS-DA models trained with spectral data from pure metal substrates with and without RDX.

B. RDX Full Spectra Model

In recent years there has been significant interest in LIBS for explosive residue detection at standoff distances [18,23–26]. We have previously demonstrated the strong dependence of the RDX residue LIBS spectra on the substrate material properties [9,13,18]. One approach to reducing the effect of the substrate would be to minimize the amount of substrate material entrained in the laser-induced plasma by selectively ablating the RDX. However, reducing the amount of ablated substrate by decreasing the laser pulse energy or choosing alternate laser wavelengths or pulse durations generally results in a significant decrease in signal-to-noise ratio for the LIBS spectra (reducing the limit of detection) and often adds to the complexity and cost for the experimental setup. Alternatively, we have been exploring the use of chemometric analysis methods such as PLS-DA to minimize spectral differences among similar samples of interest (e.g., RDX residue on different substrates) and emphasize the spectral differences between explosive and nonexplosive residues [13,18].

Previously we demonstrated the differences in the LIBS spectra of RDX resulting from the chemical reactions of RDX and metals in the laser-induced plasma [9]; for this work, a PLS-DA model was developed using the entire broadband LIBS spectra as variable inputs in order to determine if the RDX residues on the different metal surfaces could be correctly classified together. Although using the full broadband spectra in the model may be counterintuitive for explosive residue classification (which depends on only a few specific emission features), we have previously

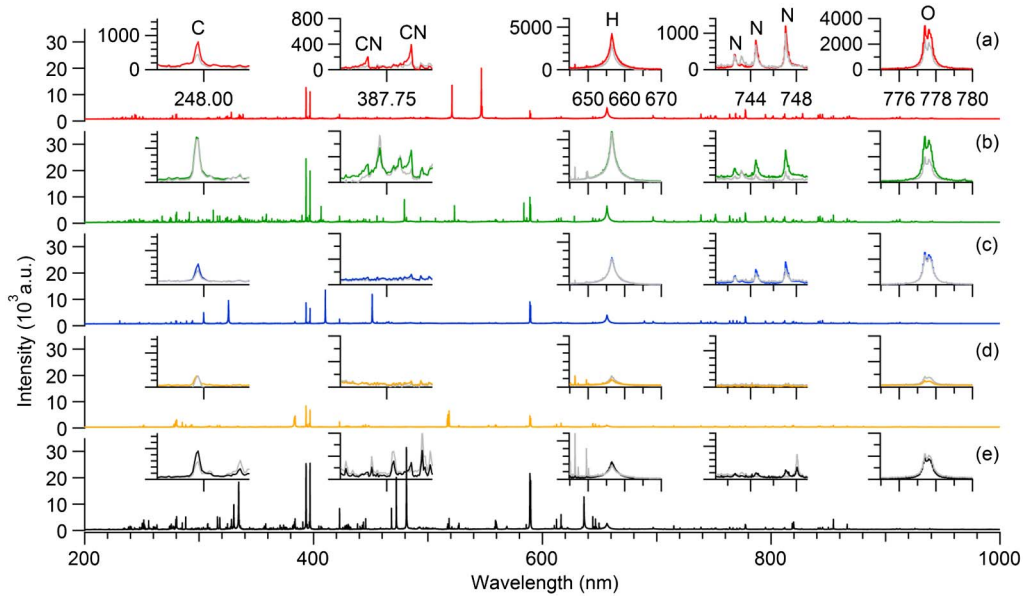

Fig. 2. (Color online) LIBS spectra of RDX residue on (a) Ag, (b) Au, (c) In, (d) Mg, and (e) Zn substrates. The insets show the emission lines due to RDX and trace organic content from the substrates. The gray lines in the insets correspond to the relevant blank substrate spectra.

shown that in many cases the broadband spectra provide a higher true positive rate (TPR) due to the complexity of the laser–material interaction [13,18]. An 11-class model consisting of one RDX class and 10 classes of pure metals (Al, Cu, Ni, Sn, Ti, Au, Mg, Zn, In, and Ag) was developed with 300 single-shot spectra and 20 latent variables. The RDX class contained spectra of RDX residue on all 10 substrates; the latent variables were thus chosen by the model to describe the differences between RDX and the blank metal substrates rather than describing the spectral differences in the RDX residue on multiple substrates. The blank metals were assigned individual classes in the PLS-DA model to increase the robustness of the model toward identifying future test samples (generally, the more classes a PLS-DA model has, the more robust it becomes).

The variable importance in projection (VIP) scores calculated by the chemometric software show which variables (e.g., spectral wavelengths) contribute to each class in the model [27]. The higher the VIP score, the more the variable contributed to the classification by the model. A comparison of the VIP scores for the Au class in a pure metal model (consisting of 10 classes with spectra from the pure metal substrates only) and the RDX residue model shows that while the scores for the Au emission lines were very similar for the two models, in the pure metal model emission lines due to organic contaminants (e.g., C and H) contributed more strongly to the

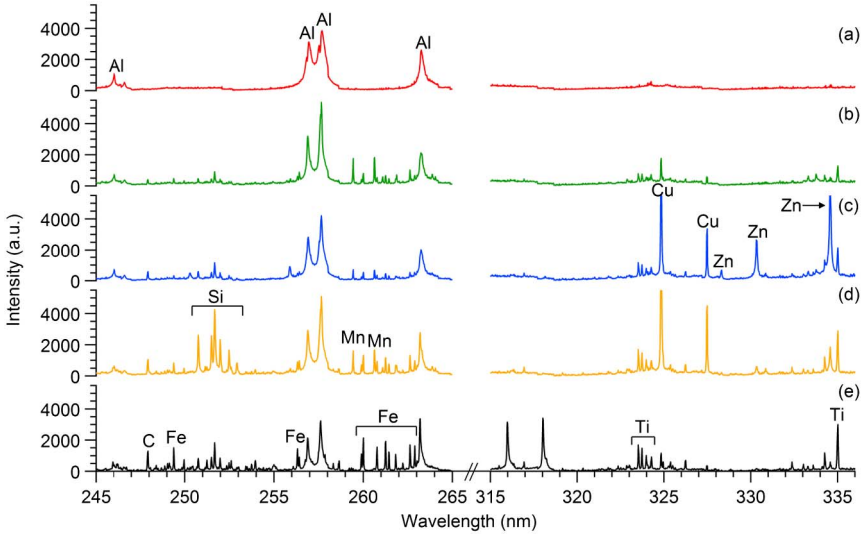

Fig. 3. (Color online) Selected spectral regions for the blank Al substrates: (a) Al (99.999%), (b) Al alloy 5182 (94.58%), (c) Al alloy 7075 (89.76%), (d) Al alloy 380 (82.99%), and (e) Al_2O_3.

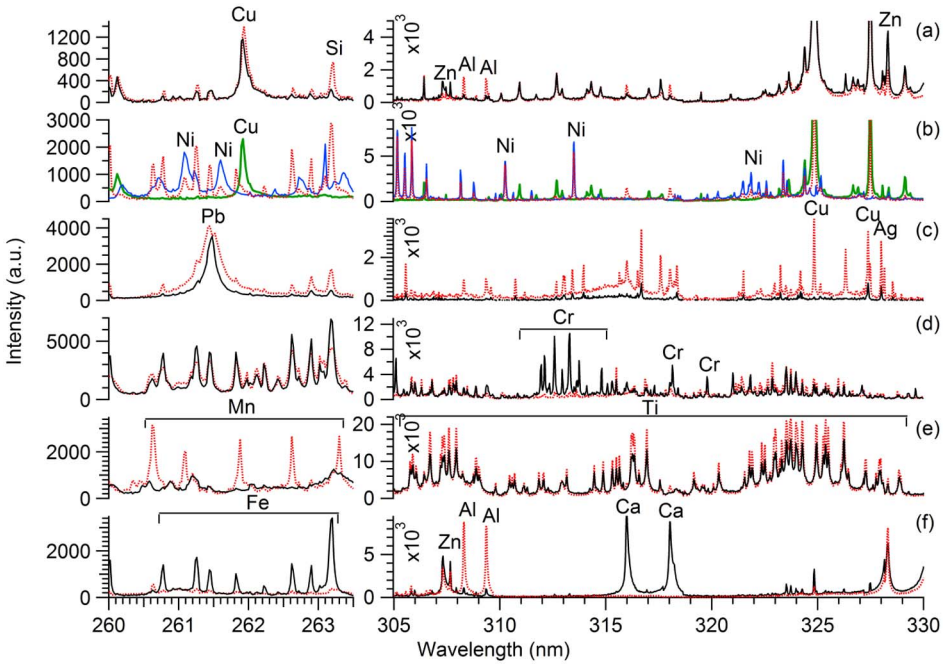

Fig. 4. (Color online) Selected spectral regions for the blank alloy substrates: (a) brass alloy 1107 (solid black) and brass alloy 1110 (dotted red); (b) Ni (solid blue), Cu (thick green), and Ni-Cu alloy C1248 (dotted red); (c) high-purity lead C2418 (solid black) and lead alloy C2417 (dotted red); (d) stainless steel C1296 (solid black) and low-alloy steel 1761A (dotted red); (e) Ti (solid black) and Ti alloy 641 (dotted red); and (f) Zn (solid black) and Zn alloy 625 (dotted red).

classification of the blank metal substrate (Fig. 5). Because the RDX classification in the residue model depends strongly on the organic emission lines, the deemphasis of the weak organic signals from the blank substrates in the RDX residue model minimizes the incorrect classification of the blank substrates with the RDX residue (i.e., false positives).

The performance of the RDX residue model was tested using an additional 400 single-shot spectra from the 10 substrates with and without RDX; these spectra were not included in the training set used to develop the model. Table 2 shows the classification results obtained for the validation test set using a threshold for classification of 35% predicted probability (this threshold gave the best model performance based on cross-validation of the training set data). The model correctly classified 95.0% of the RDX test samples (true positives), with 5.5% false positives. The In substrate was the most problematic, resulting in only 80% true positives for RDX classification and 80% false positives (four out of five spectra). An examination of the spectra revealed that while the addition of RDX residue to most of the substrates resulted in a noticeable decrease in substrate emission lines, the spectra for the In substrate with and without RDX are nearly identical [Fig. 2(c)]. In this case, the plasma chemistry is less important than other matrix effects, such as the interaction of the laser with the metal [28]. A similar effect was observed with the Mg substrate [Fig. 2(d)], which resulted in 40% false positives. The reason for the 14% false positives on the Ni substrate is likely spectral interference in the N region [Fig. 1(c)].

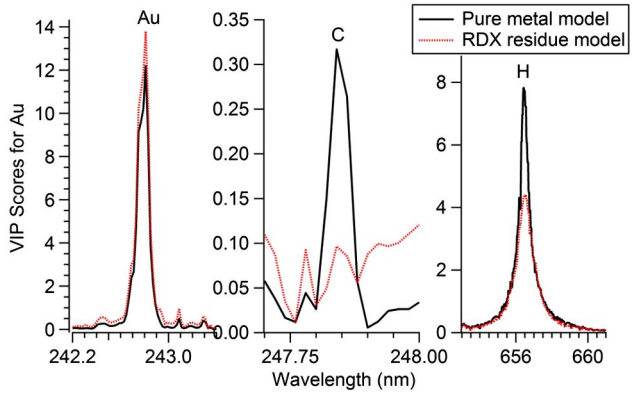

Fig. 5. (Color online) Comparison of VIP scores for the Au class in the pure metal model and the RDX residue model. The VIP scores for the Au emission lines are approximately the same for both models, while the emission lines such as C and H due to contaminants in the blank substrate are less important in the RDX residue model.

In addition to correctly classifying with RDX in the model, 26.0% of the test spectra with RDX residue were also classified with the correct class corresponding to the metal substrate. For example, 100% of the RDX residue spectra on Mg classified with RDX, and 100% of those spectra also classified with Mg. Of the blank substrate test spectra, 99.5% were correctly classified with the corresponding metallic model class, with only 0.1% misclassification.

By using the full LIBS spectra as inputs to the PLS-DA model, classification of the RDX depends not only on emission features due to the RDX but also on substrate emission lines. Figure 6 shows the VIP

Table 2. PLS-DA Results for the Classification of RDX Residue on 10 Metal Substrates Using the Full Spectra[a]

		RESPONSE										
	Validation set	RDX	Ag	Al	Au	Cu	In	Mg	Ni	Sn	Ti	Zn
TRUTH	AlRDX (35)	100%	0%	14%	0%	0%	0%	0%	0%	0%	0%	0%
	CuRDX (35)	100%	0%	0%	0%	3%	0%	0%	0%	0%	0%	0%
	NiRDX (35)	83%	0%	0%	0%	0%	0%	0%	94%	0%	0%	0%
	SnRDX (35)	91%	0%	0%	3%	0%	0%	11%	0%	0%	0%	0%
	TiRDX (35)	100%	0%	0%	0%	0%	0%	0%	11%	0%	3%	0%
	AuRDX (5)	100%	0%	0%	60%	0%	0%	0%	0%	0%	0%	0%
	MgRDX (5)	100%	0%	0%	0%	0%	0%	100%	0%	0%	0%	0%
	ZnRDX (5)	100%	0%	0%	0%	0%	0%	0%	0%	0%	0%	20%
	AgRDX (5)	100%	0%	0%	0%	0%	0%	0%	0%	0%	0%	0%
	InRDX (5)	80%	0%	0%	0%	0%	60%	0%	0%	0%	0%	0%
	Ag (5)	0%	100%	0%	0%	0%	0%	0%	0%	0%	0%	0%
	Al (35)	0%	0%	100%	0%	0%	0%	0%	0%	0%	0%	0%
	Au (5)	0%	0%	0%	100%	0%	0%	0%	0%	0%	0%	0%
	Cu (35)	0%	0%	0%	0%	100%	0%	0%	0%	0%	0%	0%
	In (5)	80%	0%	0%	0%	0%	80%	0%	0%	0%	0%	0%
	Mg (5)	40%	0%	0%	0%	0%	0%	100%	0%	0%	0%	0%
	Ni (35)	14%	0%	0%	0%	0%	0%	0%	100%	0%	0%	0%
	Sn (35)	0%	3%	0%	0%	0%	0%	0%	0%	100%	0%	0%
	Ti (35)	0%	0%	0%	0%	0%	0%	0%	0%	0%	100%	0%
	Zn (5)	0%	0%	0%	0%	0%	0%	0%	0%	0%	0%	100%

[a]Number of test spectra listed in parentheses.

scores for the RDX class in the PLS-DA model—they include numerous metal emission features. For example, the emission feature contributing most strongly to the RDX class is a relatively weak Ti I line at 521.970 nm. This feature has a signal-to-noise ratio of ~10 in the spectra of the blank substrate and only ~2 in the spectra of RDX residue on Ti; thus the presence or absence of the substrate line is used by the model as an indication of whether a residue is present. Although using the full LIBS spectra in the model typically results in better classification performance, the disadvantage for residue classification is that the classification of residues on other substrates outside the model can be significantly poorer [13]. In order to assess the ability of this model to classify RDX on other substrates, a second validation set consisting of 160 spectra acquired on aluminum alloys and 280 spectra acquired on other metal alloys was tested against the model.

The results of testing the second validation set against the RDX class in the model are shown in Table 3. The spectra with a predicted probability above the 35% threshold were classified as RDX (or the corresponding model class). The overall TPR for the alloy test set was 87.9% with 37.5% false positives. Despite the differences between the Al alloys and the pure Al in the model, 91.3% of the test spectra of RDX residue on the Al alloys were correctly classified with the RDX in the model. For most explosive-detection applications, classification of the blank substrates is only important when they incorrectly classify with the RDX. The blank Al_2O_3 substrate resulted in 100% false positives, partially because of the strong O emission lines (because O is one of the key indicators for the presence of RDX). The blank Al_2O_3 also has a strong C emission line [Fig. 3(e)], as does the Al 380 substrate [Fig. 3(d)], which has a 45% false positive rate (FPR) for RDX residue classification.

Similarly, the other metal alloy substrates with RDX residue mostly classified correctly (86.5%). However, 100% of the blank Zn 625 alloy spectra classified with the RDX. As with the In substrate, the Zn 625 substrate has strong C, H, N, and O emission features, and the spectra with and without the RDX are nearly indistinguishable. For the same reason, both brass alloys also classified significantly with RDX residue (100% and 90% for 1107 and 1110, respectively). Incorporating the spectra from the Al_2O_3 and Zn 625 substrates (along with the other validation set data) into the model training set should improve the performance of the model for RDX residue classification.

C. RDX Intensity/Ratio Model

In addition to constructing a substrate-independent PLS-DA model, a second method for improving the classification of explosive residues, based on the use of intensities and ratios, has been extensively studied by our group [1,17,29]. In this approach, only the spectral features present in the LIBS spectra of the explosive residue are input into the chemometric model, along with their corresponding intensity ratios. Table 4 lists emission features observed in the spectra of RDX; there were many more emission lines observed in the broadband spectra, however only the strongest emission lines free from interfering metal lines (from the five high-purity metal substrates) were selected for inclusion in the model. For example, the (0–0) transition of CN at 388.34 nm is significantly blended with the Ti I line at 388.29 nm and was therefore not included.

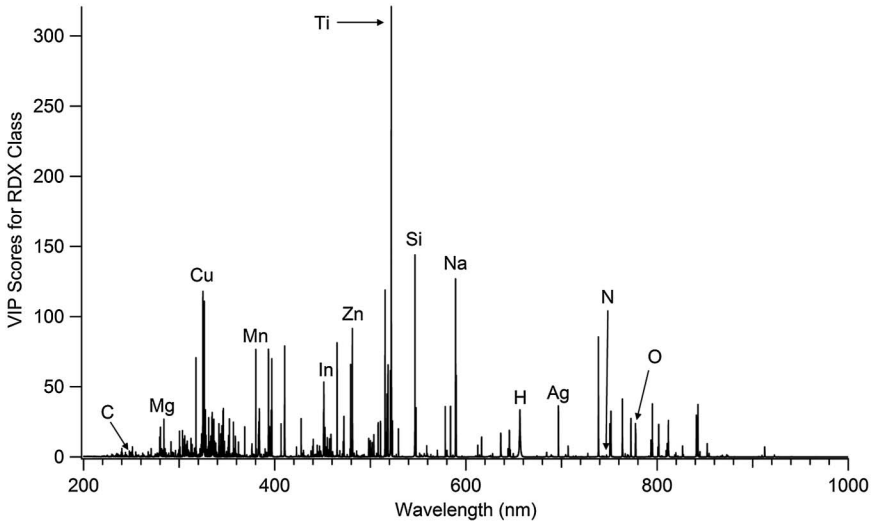

Fig. 6. VIP scores from the RDX class in the PLS-DA model for classification of RDX residues on 10 metal substrates. Emission lines from both the RDX and the substrates contribute to the classification of the RDX residue.

The emission intensities for the impurities (K, Na, Ca) were higher for RDX residue on the high-purity substrates (Al, Cu, Ni, Sn, Ti) than for the blank substrates but were higher for the blank laboratory-grade substrates (Ag, Au, In, Mg, Zn) than for the RDX residue. The Mg substrate has particularly strong C, H, N, and O emission compared to the metal emission lines [Fig. 2(d)]. The presence of the argon-bath gas minimizes the amount of O and N from the air in the plasma and provides a convenient way to normalize the emission spectra to decrease the effect of shot-to-shot variations and differing laser–material interactions. The background-corrected peak intensity of the emission lines in Table 4 were normalized to the peak intensity of the Ar line at 763.511 nm.

Compared to nonenergetic materials, most energetic materials contain higher concentrations of O and N than C and H; thus, explosive residues can be distinguished from nonenergetic materials based on the elemental ratios of those species. For this data set, a simple set of ratios was constructed based on each single-shot spectrum (C/H, C/N, C/O, C/CN, H/N, H/O, H/CN, N/O, N/CN, O/CN), although more complex ratios can be used to improve the classification for more practical models with multiple residues [29]. The emission lines shown in bold in Table 4 were used to calculate the ratios. The plasma excitation temperature was calculated based on the Ar lines at 750.387 and 751.465 nm with the Boltzmann two-line method [9] and used as a variable input as well, giving a total of 35 variables per spectrum.

An 11-class PLS-DA model (with the same classes as the full spectra model in Section 3.B) was

Table 3. PLS-DA Results for the Second Validation Test Set Consisting of Substrates Not Included in the Full Spectra Model[a]

		RESPONSE
	Alloy test set	RDX
TRUTH	Al_2O_3 (20)	**100%**
	Al_2O_3+RDX (20)	**100%**
	Al 380 (20)	**45%**
	Al 380+RDX (20)	**90%**
	Al 7075 (20)	0%
	Al 7075+RDX (20)	**100%**
	Al 5182 (20)	0%
	Al 5182+RDX (20)	**75%**
	Lead C2417 (20)	**5%**
	Lead C2417+RDX (20)	**55%**
	Lead C2418 (20)	**65%**
	Lead C2418+RDX (20)	**80%**
	Ni-Cu alloy (20)	**5%**
	Ni-Cu alloy+RDX (20)	**85%**
	Steel 1761a (20)	0%
	Steel 1761a+RDX (20)	**60%**
	Steel C1296 (20)	**15%**
	Steel C1296+RDX (20)	**95%**
	Ti 641 (20)	0%
	Ti 641+RDX (20)	**100%**
	Zn 625 (20)	**100%**
	Zn 625+RDX (20)	**100%**
	Alloy L-605 (20)	0%
	Alloy L-605+RDX (20)	**90%**
	Brass 1107 (20)	**100%**
	Brass 1107+RDX (20)	**100%**
	Brass 1110 (20)	**90%**
	Brass 1110+RDX (20)	**100%**

[a]Number of test spectra listed in parentheses.

Table 4. Selected Emission Features Based on Intensity and Lack of Spectral Interferences

Species	Selected Emission Features (Wavelengths from [30])
C	**247.856**, 906.143, 909.483, 940.573, 962.080
H	**656.285**
N	744.229, **821.634**, 824.239
O	715.670, **777.194**, 777.417, 844.636, 882.043, 926.601
CN	**387.14**
K	766.490, 769.896
Na	588.995, 589.592, 819.482
Ca	315.887, 393.366, 422.673

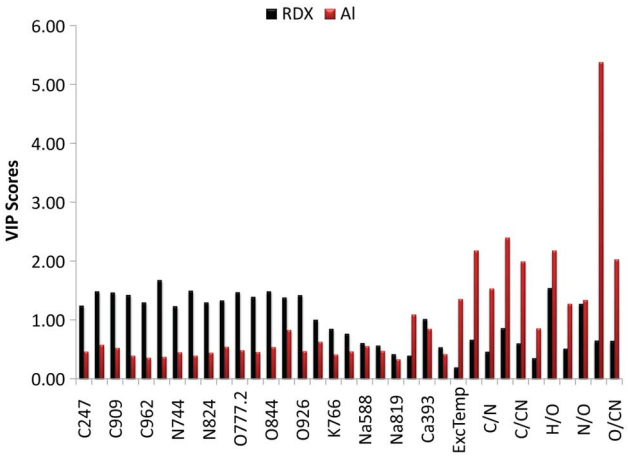

Fig. 7. (Color online) VIP scores for the RDX and Al classes using a model based on selected emission intensities, calculated excitation temperature, and selected intensity ratios. For clarity, not all of the variable names are displayed on the x axis.

constructed with the same spectra used to train the full spectra model; however, this time only the 35 variables described above were used as the inputs for the model. Twenty latent variables were selected to capture the variance in the training set. Figure 7 compares the VIP scores used to classify the RDX residue and one of the blank substrates (Al). The emission intensities of the C, H, N, and O are more influential for describing the RDX class, as expected, while the impurity intensities (Ca, Na, K) contribute fairly equally to both classes. The excitation temperatures more strongly influence the blank substrate classification because the substrates covered in RDX residue have similar temperatures [9]. The ratios are more important for the classification of the blank substrate in this model; the ratios would be essential for discriminating multiple similar organic residues in a more complex model [29].

As before, the model was tested with a validation set consisting of spectra not used to train the model (Table 5). The use of specific emission intensities and ratios significantly improved the overall TPR (96.5%) and FPR (1.0%) for explosive classification; however, the correct classification of the blank substrates was significantly lower (91.0%). This result is entirely expected as no metal emission lines were used in the model. In general, for explosive residue detection, the only important question is whether the analyzed material is explosive or nonexplosive. The false positives for the blank Mg substrate are a result of the relatively strong C, H, N, and O emission present in some of the spectra.

The results from testing the second validation set of metal alloys against the intensity/ratio PLS-DA model are shown in Table 6. Once again, using the specific intensities and ratios increased the TPR (88.9%) and decreased the FPR (30.7%). As with the first validation set, the classification of the metal-alloy test spectra with the blank metal substrate classes is essentially meaningless as only the variables related to the RDX residue are considered by the model.

D. RDX Fusion Model

Although the TPRs for the models described in Sections 3.B and 3.C were quite high (95.0% and 96.5%, respectively) given the disparities in the RDX residue spectra on the different substrates, the relatively high FPRs (especially for the unknown substrates) would be unacceptable in an explosive detection application. A third approach to improving

Table 5. PLS-DA Results for the Classification of RDX Residue on 10 Metal Substrates Using the Intensities/Ratio Model[a]

		RESPONSE										
	Validation set	RDX	Ag	Al	Au	Cu	In	Mg	Ni	Sn	Ti	Zn
TRUTH	Al+RDX (35)	**100%**	3%	**0%**	3%	0%	9%	3%	0%	0%	0%	6%
	Cu+RDX (35)	**100%**	0%	0%	0%	**0%**	0%	11%	0%	0%	0%	0%
	Ni+RDX (35)	**100%**	14%	11%	20%	0%	0%	0%	**0%**	0%	0%	0%
	Sn+RDX (35)	**94%**	0%	0%	0%	0%	3%	14%	6%	**0%**	0%	0%
	Ti+RDX (35)	**89%**	3%	0%	0%	9%	0%	11%	11%	0%	**3%**	0%
	Au+RDX (5)	**100%**	0%	0%	**0%**	0%	0%	0%	0%	0%	0%	0%
	Mg+RDX (5)	**100%**	0%	0%	0%	0%	0%	**60%**	0%	0%	0%	0%
	Zn+RDX (5)	**100%**	0%	0%	0%	0%	20%	40%	0%	0%	0%	**20%**
	Ag+RDX (5)	**100%**	**0%**	0%	0%	0%	0%	0%	0%	0%	0%	0%
	In+RDX (5)	**80%**	0%	0%	0%	0%	**60%**	20%	0%	0%	0%	0%
	Ag (5)	0%	**100%**	0%	0%	20%	0%	0%	0%	0%	0%	0%
	Al (35)	0%	23%	**100%**	17%	23%	3%	0%	0%	3%	0%	0%
	Au (5)	0%	0%	20%	**100%**	0%	0%	0%	0%	0%	0%	0%
	Cu (35)	0%	66%	3%	0%	**54%**	0%	0%	86%	0%	0%	0%
	In (5)	0%	20%	0%	0%	0%	**100%**	0%	0%	0%	0%	0%
	Mg (5)	40%	0%	0%	20%	0%	0%	**100%**	20%	0%	0%	0%
	Ni (35)	0%	11%	0%	0%	14%	0%	0%	**94%**	0%	0%	0%
	Sn (35)	0%	14%	11%	0%	20%	0%	9%	0%	**100%**	0%	3%
	Ti (35)	0%	0%	3%	0%	0%	0%	0%	0%	0%	**100%**	0%
	Zn (5)	0%	0%	0%	0%	0%	0%	0%	0%	0%	0%	**100%**

[a]Number of test spectra listed in parentheses.

Table 6. PLS-DA Results for the Second Validation Test Set Consisting of Substrates Not Included in the Intensity/Ratio Model[a]

		RESPONSE
	Alloy test set	RDX
TRUTH	Al_2O_3 (20)	85%
	Al_2O_3+RDX (20)	**100%**
	Al 380 (20)	20%
	Al 380+RDX (20)	**90%**
	Al 7075 (20)	0%
	Al 7075+RDX (20)	**80%**
	Al 5182 (20)	0%
	Al 5182+RDX (20)	**70%**
	Lead C2417 (20)	50%
	Lead C2417+RDX (20)	**95%**
	Lead C2418 (20)	25%
	Lead C2418+RDX (20)	**70%**
	Ni-Cu alloy (20)	10%
	Ni-Cu alloy+RDX (20)	**95%**
	Steel 1761a (20)	5%
	Steel 1761a+RDX (20)	**85%**
	Steel C1296 (20)	45%
	Steel C1296+RDX (20)	**75%**
	Ti 641 (20)	0%
	Ti 641+RDX (20)	**100%**
	Zn 625 (20)	0%
	Zn 625+RDX (20)	**90%**
	Alloy L-605 (20)	85%
	Alloy L-605+RDX (20)	**100%**
	Brass 1107 (20)	10%
	Brass 1107+RDX (20)	**100%**
	Brass 1110 (20)	95%
	Brass 1110+RDX (20)	**95%**

[a]Number of test spectra listed in parentheses.

the classification of explosive residues based on fusing the two types of models (full spectra and selected intensities/ratios) has been demonstrated by our group for several varied data sets [13,18,29,31]. Briefly, the probability that each test spectrum belongs to a particular class in the full spectra model is multiplied by the probability that the spectrum belongs to the same class in the intensity/ratio model. A new, lower threshold (e.g., $0.35 \times 0.35 = 0.12$) is chosen to determine class membership. In this way, only samples that register as positive for explosives in both models fall above the new threshold for classification. Receiver operating characteristic (ROC) curves were generated for each of the models by varying the threshold (Fig. 8). A perfect explosives detector would have an ROC curve with a data point at 100% correct classification (or TPR) and 0% misclassification (or FPR).

Figure 8 compares the results from testing of the two models described in Sections 3.B and 3.C; the ROC curves for the classification of the RDX residue in the validation set and in the alloy test set are shown for each model. In both cases, the fusion approach improves the ROC curve performance, although the improvement is much more significant for the alloy test set. The improvement in TPR and

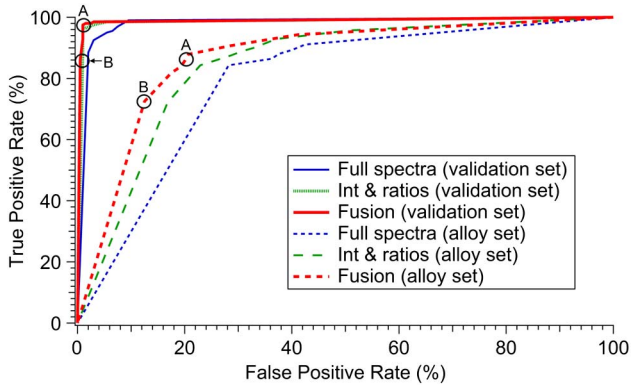

Fig. 8. (Color online) ROC curves for the classification of the RDX residue (from the validation and alloy sets) using PLS-DA models based on full spectra, selected intensities/ratios, and fused probabilities. The points on the fusion ROC curves labeled A correspond to a threshold of 0.12, while the points labeled B correspond to a threshold of 0.56.

FPR achieved depends on the threshold selection (i.e., position on the ROC curve) and on the application requirements. With a threshold of 0.12, the TPR for the validation test set is 97.5% and the FPR is 1.0% for the fusion model (and the FPR for the alloy test set is decreased to 20.0%). If minimizing the number of false positives is most important, a higher threshold for classification can be selected at the expense of the TPR (e.g., a threshold of 0.56 gives a TPR of 86.0% and an FPR of 0.5% for the validation test set and an FPR of 12.5% for the alloy test set).

4. Conclusions

By down-selecting the full spectral data to those features pertaining to the RDX residue, we were able to improve the TPR (from 95.0% to 96.5%) and significantly reduce the FPR (from 5.5% to 1.0%). This outcome is in contrast to our earlier results, which showed an improvement in both TPR and FPR using full broadband spectra instead of intensities/ratios for residue classification on substrates included in the model [13,18]. The biggest difference in the current study is the dramatic effect of the metallic substrates on the plasma chemistry of the ablated RDX residue and the subsequent effects on the LIBS spectra of the explosive residues. The fact that whether the full broadband spectra or selected intensities/ratios provide the best residue classification depends on the substrate composition suggests that although the information in the two models may be highly correlated, individually neither type of model adequately captures all of the information available from the spectral signatures.

The FPRs for a second test set consisting of metal alloys, which cause distinct differences in the plasma chemistry of the ablated RDX residue not accounted for in the model, were unacceptably high for both types of models (>30%). The fusion model, which combines the probabilities obtained in the full spectra model and the intensity/ratio model, results in a modest improvement in the TPR (depending on

the chosen threshold) and a significant reduction in the FPR, especially for the substrates not included in the model training sets (down to 20.0% with a threshold of 0.12 and 12.5% with a threshold of 0.56). This result is consistent with previous explosive residue studies [13,18].

Despite the distinct differences in the LIBS spectra of RDX residue on metallic substrates, we have shown that the RDX residues can be classified independent of substrate with a high degree of success. Although we do not claim that the limited models presented here would enable explosive residue detection in a realistic environment, together with our previous studies these results provide valuable insight into the best approaches for the development of explosive detection systems based on LIBS. Future improvements to the models presented here could consist of incorporating the validation set data (including the metal alloys) into the training set for the models, increasing the number of organic emission intensities selected, and creating more complex ratios. In addition, models containing a more varied set of substrates (e.g., organic and metallic) should be developed as clear differences in the chemometric results based on substrate type have been demonstrated.

References

1. J. L. Gottfried, F. C. De Lucia, Jr., C. A. Munson, and A. W. Miziolek, "Laser-induced breakdown spectroscopy for detection of explosives residues: a review of recent advances, challenges, and future prospects," Anal. Bioanal. Chem. **395**, 283–300 (2009).
2. D. A. Cremers and L. J. Radziemski, *Handbook of Laser-Induced Breakdown Spectroscopy* (Wiley, 2006).
3. V. I. Babushok, F. C. De Lucia, Jr., P. J. Dagdigian, J. L. Gottfried, C. A. Munson, M. J. Nusca, and A. W. Miziolek, "Kinetic modeling study of the laser-induced plasma plume of cyclotrimethylenetrinitramine (RDX)," Spectrochim. Acta B **62**, 1321–1328 (2007).
4. V. Lazic, A. Palucci, S. Jovicevic, C. Poggi, and E. Buono, "Analysis of explosive and other organic residues by laser induced breakdown spectroscopy," Spectrochim. Acta B **64**, 1028–1039 (2009).
5. P. J. Dagdigian, A. Khachatrian, and V. I. Babushok, "Kinetic model of C/H/N/O emissions in laser-induced breakdown spectroscopy of organic compounds," Appl. Opt. **49**, C58–C66 (2010).
6. P. Lucena, A. Dona, L. M. Tobaria, and J. J. Laserna, "New challenges and insights in the detection and spectral identification of organic explosives by laser induced breakdown spectroscopy," Spectrochim. Acta B **66**, 12–20 (2011).
7. M. Civiš, S. Civiš, K. N. Sovová, K. Dryahina, P. Španěl, and M. Kyncl, "Laser ablation of FOX-7: proposed mechanism of decomposition," Anal. Chem. **83**, 1069–1077 (2011).
8. F. C. De Lucia, Jr. and J. L. Gottfried, "Characterization of a series of nitrogen-rich molecules using laser-induced breakdown spectroscopy," Propellants Explos. Pyrotech. **35**, 268–277 (2010).
9. J. L. Gottfried, "Laser-induced plasma chemistry of the explosive RDX with various metallic nanoparticles," Appl. Opt. **51**, B13–B21 (2012).
10. D. A. Cremers and R. C. Chinni, "Laser-induced breakdown spectroscopy: capabilities and limitations," Appl. Spectrosc. Rev. **44**, 457–506 (2009).
11. C. Chaleard, P. Mauchien, N. Andre, J. Uebbing, J. L. Lacour, and C. Geersten, "Correction of matrix effects in quantitative elemental analysis with laser ablation optical emission spectrometry," J. Anal. At. Spectrom. **12**, 183–188 (1997).
12. S. Laville, M. Sabsabi, and F. R. Doucet, "Multi-elemental analysis of solidified mineral melt samples by laser-induced breakdown spectroscopy coupled with a linear multivariate calibration," Spectrochim. Acta B **62**, 1557–1566 (2007).
13. J. L. Gottfried, F. C. De Lucia, Jr., and A. W. Miziolek, "Discrimination of explosive residues on organic and inorganic substrates using laser-induced breakdown spectroscopy," J. Anal. At. Spectrom. **24**, 288–296 (2009).
14. E. Tognoni, G. Cristoforetti, S. Legnaioli, and V. Palleschi, "Calibration-free laser-induced breakdown spectroscopy: state of the art," Spectrochem. Acta B **65**, 1–14 (2010).
15. V. Lazic, A. Palucci, S. Jovicevic, and M. Carpanese, "Detection of explosives in traces by laser induced breakdown spectroscopy: differences from organic interferents and conditions for a correct classification," Spectrochim. Acta B **66**, 644–655 (2011).
16. D. W. Hahn and N. Omenetto, "Laser-induced breakdown spectroscopy (LIBS), part II: review of instrumental and methodological approaches to material analysis and applications to different fields," Appl. Spectrosc. **66**, 347–419 (2012).
17. J. L. Gottfried, F. C. De Lucia, Jr., C. A. Munson, and A. W. Miziolek, "Strategies for residue explosives detection using laser-induced breakdown spectroscopy," J. Anal. At. Spectrom. **23**, 205–216 (2008).
18. F. C. De Lucia, Jr. and J. L. Gottfried, "Classification of explosive residues on organic substrates using laser induced breakdown spectroscopy," Appl. Opt. **51**, B83–B92 (2012).
19. Q. Wang, P. Jander, C. Fricke-Begemann, and R. Noll, "Comparison of 1064 nm and 266 nm excitation of laser-induced plasmas for several types of plastics and one explosive," Spectrochim. Acta B **63**, 1011–1015 (2008).
20. D. M. Wong and P. J. Dagdigian, "Comparison of laser-induced breakdown spectra of organic compounds with irradiation at 1.5 and 1.064 micron," Appl. Opt. **47**, G149–G157 (2008).
21. M. Barker and W. Rayens, "Partial least squares for discrimination," J. Chemom. **17**, 166–173 (2003).
22. V. I. Babushok, F. C. De Lucia, Jr., J. L. Gottfried, C. A. Munson, and A. W. Miziolek, "Double pulse laser ablation and plasma: laser induced breakdown spectroscopy signal enhancement," Spectrochim. Acta B **61**, 999–1014 (2006).
23. J. L. Gottfried, F. C. De Lucia, Jr., C. A. Munson, and A. W. Miziolek, "Double-pulse standoff laser-induced breakdown spectroscopy for versatile hazardous materials detection," Spectrochim. Acta B **62**, 1405–1411 (2007).
24. C. Lopez-Moreno, S. Palanco, J. Javier Laserna, F. C. De Lucia, Jr., A. W. Miziolek, J. Rose, R. A. Walters, and A. I. Whitehouse, "Test of a stand-off laser-induced breakdown spectroscopy sensor for the detection of explosive residues on solid surfaces," J. Anal. At. Spectrom. **21**, 55–60 (2006).
25. F. C. De Lucia, Jr., J. L. Gottfried, C. A. Munson, and A. W. Miziolek, "Multivariate analysis of standoff laser-induced breakdown spectroscopy spectra for classification of explosive-containing residues," Appl. Opt. **47**, G112–G121 (2008).
26. R. Gonzalez, P. Lucena, L. M. Tobaria, and J. J. Laserna, "Standoff LIBS detection of explosive residues behind a barrier," J. Anal. At. Spectrom. **24**, 1123–1126 (2009).
27. I.-G. Chong and C.-H. Jun, "Performance of some variable selection methods when multicollinearity is present," Chemom. Intell. Lab. Syst. **78**, 103–112 (2005).
28. J. A. Aguilera, C. Aragón, V. Madurga, and J. Manrique, "Study of matrix effects in laser induced breakdown spectroscopy on metallic samples using plasma characterization by emission spectroscopy," Spectrochim. Acta B **64**, 993–998 (2009).
29. F. C. De Lucia, Jr. and J. L. Gottfried, "Influence of variable selection on partial least squares discriminant analysis models for explosive residue discrimination," Spectrochim. Acta B **66**, 122–128 (2011).
30. Y. Ralchenko, A. E. Kramida, J. Reader, and N. A. Team, "NIST atomic spectra database (version 4.1)," http://physics.nist.gov/asd.
31. J. L. Gottfried, "Discrimination of biological and chemical threats in residue mixtures on multiple surfaces," Anal. Bioanal. Chem. **400**, 3289–3301 (2011).

NO. OF COPIES	ORGANIZATION
1 (PDF)	DEFENSE TECHNICAL INFORMATION CTR DTIC OCA 8725 JOHN J KINGMAN RD STE 0944 FORT BELVOIR VA 22060-6218
1 (PDF)	DIRECTOR US ARMY RESEARCH LAB RDRL CIO LL 2800 POWDER MILL RD ADELPHI MD 20783-1197
1 (PDF)	GOVT PRINTG OFC A MALHOTRA 732 N CAPITOL ST NW WASHINGTON DC 20401
1 (PDF)	RDRL WML B J GOTTFRIED

INTENTIONALLY LEFT BLANK.